MATERIALS CHEMISTRY FRONTIERS

RESEARCH ARTICLE

View Article Online
View Journal | View Issue

Cite this: *Mater. Chem. Front.*, 2023, **7**, 5413

TADF emitters based on a tri-spiral acridine donor and a spiro-*B*-heterotriangulene acceptor with high horizontal dipole orientation ratios and high efficiencies in deep-blue OLEDs†

Young Hoon Lee, ‡[ac] Jeoungmin Ji, ‡[b] Thi Quyen Tran, [a] Taehwan Lee, [a] Jaehoon Jung, [a] Youngil Lee, *[ac] Seunghyup Yoo *[b] and Min Hyung Lee *[a]

Received 8th June 2023,
Accepted 24th August 2023

DOI: 10.1039/d3qm00653k

rsc.li/frontiers-materials

Developing thermally activated delayed fluorescence (TADF) emitters showing high horizontal transition dipole orientation and molecular rigidity is crucial for enhancing the color purity and performance of deep-blue organic light-emitting diodes (OLEDs). Here, we report two linearly expanded TADF emitters, O-tsAC-BAsBP (**1**) and S-tsAC-BAsBP (**2**), based on a tri-spiral acridine donor and a spiro-fluorenyl *B*-heterotriangulene acceptor. These emitters exhibit deep-blue emissions, with peaks centered at 458–467 nm for **1** and 462–469 nm for **2**, respectively, in the host films, with high photoluminescence quantum yields, small singlet–triplet energy splitting ($\Delta E_{ST} < 0.05$ eV), and short delayed fluorescence lifetimes ($\tau_d < 2$ μs). Theoretical studies demonstrate that effective spin–orbit coupling between the charge transfer singlet (^{1}CT) and acceptor-centered local triplet (^{3}LE) excited states accelerates the reverse intersystem crossing (RISC) process, resulting in a high RISC rate constant of $\sim 10^6$ s^{-1}. Notably, both emitters exhibit very high horizontal dipole orientation ratios ($\Theta_{\parallel}$) of ~93% in their doped host films. Owing to the outstanding TADF characteristics and high $\Theta_{\parallel}$ values, TADF-OLEDs incorporating emitters **1** and **2** achieve high maximum external quantum efficiencies of 27.4% and 31.5%, respectively, in the deep-blue region.

Introduction

Organic thermally activated delayed fluorescence (TADF) materials have attracted ever-growing attention as promising emissive materials in organic light-emitting diodes (OLEDs) because they can effectively harvest triplet excitons through a reverse intersystem crossing (RISC) process, thereby achieving 100% internal quantum efficiency (IQE) in OLEDs.[1–7] In general, TADF emitters are composed of donor (D) and acceptor (A) units with a largely twisted D–A structure. The D and A segments possess the well-separated HOMO and LUMO, respectively, leading to a small energy gap between the S_1 and T_1 states (ΔE_{ST}). This enables TADF emitters to undergo a fast RISC process. In addition to the IQE, the light-outcoupling efficiency (η_{out}) of a device is another key parameter that governs the external quantum efficiency (EQE) of the device.[8] Accordingly, achieving a high η_{out} is necessary to boost the EQE of OLED devices. Many studies reveal that η_{out} can be significantly improved if the horizontal orientation ratio ($\Theta_{\parallel}$) of the transition dipole moment (TDM) is above the value corresponding to the completely random orientation case ($\Theta_{\parallel}$ = 67%). Note that the majority of light is emitted in a direction perpendicular to the TDM vector. Therefore, a significant portion of light emitted from the horizontally oriented TDM can be directly outcoupled to air instead of being coupled to wave guided modes (Fig. S1 in the ESI† for the illustrative description). Hence, a high $\Theta_{\parallel}$ in the emissive layer in OLEDs can be highly beneficial for improving the EQE without the need for a separate outcoupling structure.[9–11] The factors influencing $\Theta_{\parallel}$ include, but are not limited to, molecular shapes or the presence of certain functional groups that promote the anisotropic molecular arrangement during deposition.[12] For instance, TADF emitters in a linear or a planar shape have shown high $\Theta_{\parallel}$ and, as a result, exhibited high electroluminescence (EL) performances.[13–15] However, the elongated molecular conjugation and expanded molecular

[a] *Department of Chemistry, University of Ulsan, Ulsan 44776, Republic of Korea. E-mail: lmh74@ulsan.ac.kr*
[b] *School of Electrical Engineering, KAIST, Daejeon 34141, Republic of Korea. E-mail: syoo.ee@kaist.edu*
[c] *Chemical Industry Research Institution, University of Ulsan, Ulsan, 44776, Republic of Korea. E-mail: nmryil@ulsan.ac.kr*

† Electronic supplementary information (ESI) available: Electronic Supplementary Information is available from the Royal Society of Chemistry or from the author. General information about the experimental, photophysical data, computational details, and electroluminescence results. See DOI: https://doi.org/10.1039/d3qm00653k

‡ These authors contributed equally to this work.

plane can often compromise the emission color and efficiency of TADF emitters due to various internal D–A interaction strengths or strong molecular interactions in the aggregated state.[16,17]

To address this issue, spiro-shaped donors and acceptors have been introduced into the D–A backbone to enhance the $\Theta_{\parallel}$ values without causing serious emission quenching, thanks to large steric hindrance of the spiro-groups.[18–21] Among the donors, spiro-acridine (sAC) groups have been reported to increase the molecular rigidity and $\Theta_{\parallel}$ values of the emitters.[22–25] These are also effective in lowering the HOMO energy level due to the relatively weak electron-donating ability caused by a weak hyper-conjugation effect.[21] Particularly, when combined with boron-based acceptors, TADF emitters containing sAC donors have demonstrated outstanding performances in blue OLEDs that demand the emitters with high molecular stability.[18,24,26] Furthermore, tri-spiral acridine (tsAC), which is a more structurally reinforced sAC derivative, has been recently employed in blue emitters. These emitters exhibited high molecular rigidity, an improved PLQY, and a high $\Theta_{\parallel}$ value of ~90%.[15,26] Meanwhile, TADF emitters incorporating spiro-type acceptor units have rarely been reported.[18,27–29] A representative example of such acceptors is spiro-fluorenyl-*B*-heterotriangulene, which exhibits high structural stability due to the presence of fully tethered aryl groups around the boron center.[30,31] The resulting D–A-type TADF emitters with the spiro-fluorenyl-*B*-heterotriangulene unit exhibited blue emissions with near-unity PLQYs and high $\Theta_{\parallel}$ values of ~90%, irrespective of the presence of a spiro-donor unit.[30]

Taking these into account, we herein report two linearly expanded TADF emitters, O-tsAC-BAsBP (**1**) and S-tsAC-BAsBP (**2**), composed of a tri-spiral acridine (tsAC) donor and a spiro-fluorenyl-*B*-heterotriangulene (BAsBP) acceptor to enhance the light-outcoupling efficiency in blue OLEDs. The presence of bulky spiral D and A moieties in **1** and **2** is also expected to increase both the molecular rigidity and steric hindrance, thereby effectively reducing intermolecular interactions. We found that both emitters showed deep-blue emissions with excellent TADF characteristics in the doped host films. These emitters exhibited near-unity PLQYs, small singlet–triplet energy splitting ($\Delta E_{ST} < 0.05$ eV), short delayed fluorescence lifetimes ($\tau_d < 2$ μs), and fast RISC ($k_{RISC} \sim 10^6$ s^{-1}). Remarkably, both emitters exhibited very high $\Theta_{\parallel}$ values of ~93%, which is the highest among the emitters containing spiro-acridine donors. Thanks to their outstanding TADF characteristics and high $\Theta_{\parallel}$ values, the corresponding TADF-OLEDs displayed high maximum EQEs of 27%–31% in the deep-blue region.

Results and discussion

Synthesis and characterization

Two D–A compounds, O-tsAC-BAsBP (**1**) and S-tsAC-BAsBP (**2**), were synthesized following the procedures depicted in Scheme 1. The oxygen-bridged acridine donor (O-tsACH, **1e**) was newly prepared using a modified reaction pathway based on the synthesis of the sulfur-bridged, tri-spiral acridine donor (S-tsACH, **2e**).[15] The final products (**1** and **2**) were obtained in high yields through Buchwald-Hartwig amination reactions between the X-tsACH (X = O, S) donors and a bromo-substituted spiro-fluorenyl *B*-heterotriangulene acceptor (Br-BAsBP).[30] Both compounds were analyzed by ^{1}H NMR spectroscopy and elemental analyses, while ^{11}B and ^{13}C NMR spectra of the compounds could not be obtained due to the poor solubility in organic solvents (Fig. S2–S7, ESI†). These compounds were chemically stable in solution and solid states under ambient conditions and also displayed high thermal stability evidenced by their elevated decomposition temperatures (T_{d5} = 466 °C for

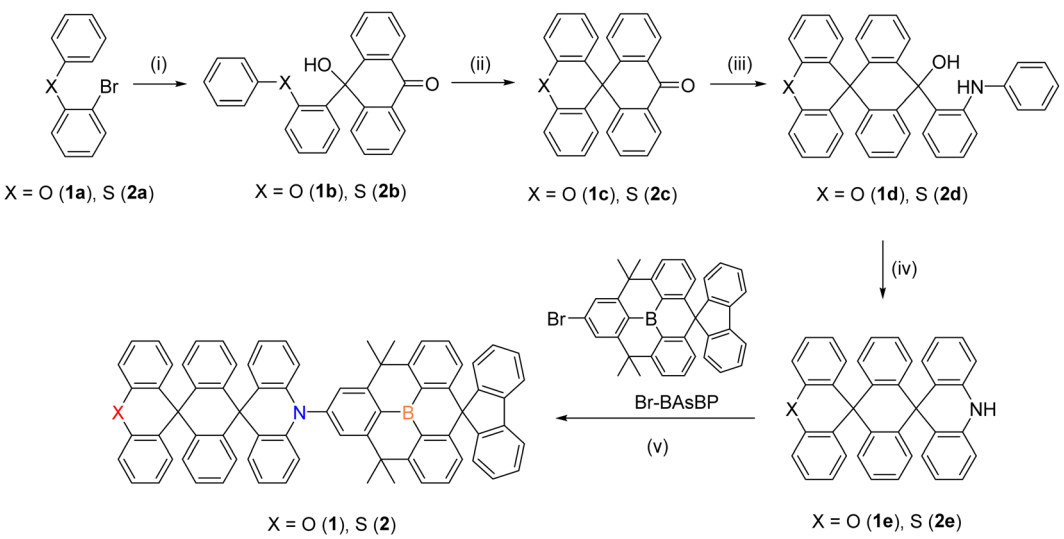

Scheme 1 Conditions: (i) *n*-BuLi, THF, −78 °C, then 1.0 M HCl, MeOH, and RT. (ii) c-HCl, AcOH, and reflux. (iii) *n*-BuLi, THF, −78 °C, then 1.0 M HCl, MeOH, and RT. (iv) c-HCl, AcOH, and reflux. (v) Pd(*t*-$Bu_3P)_2$, Br-BAsBP, *t*-BuONa, toluene, and reflux.

1 and 464 °C for **2** at 5% weight loss). Notably, the T_{d5} values were superior to that of the reference compound, sAC-BAsBP (**3**, T_{d5} = 420 °C), which consisted of mono spiro-donor and spiro-acceptor units (Fig. S8, ESI†).[30] This result indicates that the tri-spiral skeleton can greatly improve the thermal stability of boron-based D–A compounds.

Photophysical properties

The UV/Vis absorption and photoluminescence (PL) spectra of **1** and **2** were first obtained in toluene at room temperature (Fig. 1 and Table 1). In addition, the absorption spectra of the donor (X-tsACH; X = O or S) and acceptor (HBAsBP) molecules were recorded to understand the electronic transition of **1** and **2** (Fig. S9, ESI†). The intense absorption in the high-energy region of 270–350 nm was attributable to the local π–π* states of the D and A units.[32,33] The broad and weak absorption in the low-energy region of 350–450 nm is assigned to the intramolecular charge transfer (ICT) transition from the D to A units (Fig. 1b and Table 1). The similar absorption onset of both compounds resulted in a comparable HOMO–LUMO energy gap (E_g) of 2.93 eV, slightly higher in energy than that of sAC-BAsBP (**3**, 2.91 eV).[30] This finding supports the blue-shifted emission of **1** and **2** compared to that of **3** (see below). Compounds **1** and **2** underwent X-tsAC (X = O, S)-centered irreversible oxidations with onset oxidation potentials of 0.54 V for **1** and 0.52 V for **2**, respectively (Fig. S10, ESI†). Accordingly, the comparable HOMO energy levels were determined to be −5.34 eV for **1** and −5.32 eV for **2**, respectively. In combination with the E_g values and HOMO levels, the LUMO energy levels of −2.41 eV for **1** and −2.39 eV for **2**, respectively were deduced. These results indicate that the O- and S-containing tsAC donors have similar electronic effects on the HOMO and LUMO presumably due to substitution of the O and S atoms at a distal position. Both compounds displayed deep-blue emissions with a peak centered at 457 nm in their PL spectra, and their broad and structureless emissions originated from an ICT transition (Fig. 1b). These compounds exhibited decent photoluminescence quantum yields (PLQYs) of 70–74% in deoxygenated toluene, whereas the PLQYs were dramatically dropped to 31% with a decrease in the PL intensity in oxygen-saturated toluene, as a result of the triplet state quenching by oxygen (Fig. S11, ESI†). The transient PL decay traces at room temperature displayed characteristic prompt (τ_p) and delayed (τ_d) components, with a τ_p value of 20 ns and a τ_d value of 5.83–7.50 μs, respectively (Fig. 1c). Next, the photophysical properties of 20 wt%-doped films of **1** and **2** in a DPEPO host matrix were investigated (Fig. 1d). The PL spectra featured deep-blue emissions centered at 467 nm (**1**) and 469 nm (**2**), respectively, which were red-shifted compared to those obtained in toluene. The redshifts can be primarily attributed to the increased polarity of the host matrix, which stabilizes the CT excited state.[34,35] The PLQYs and full width at half maximums (FWHMs) for the films were 100% and 63 nm for **1**, and 84% and 66 nm for **2**, respectively. The increased PLQY and narrower FWHM of the films compared with the results in toluene (PLQY = 70–74%, FWHM = 69 nm) can be attributed to the suppressed intramolecular vibrations and rotations in the rigid state.[36] The fluorescence and phosphorescence spectra

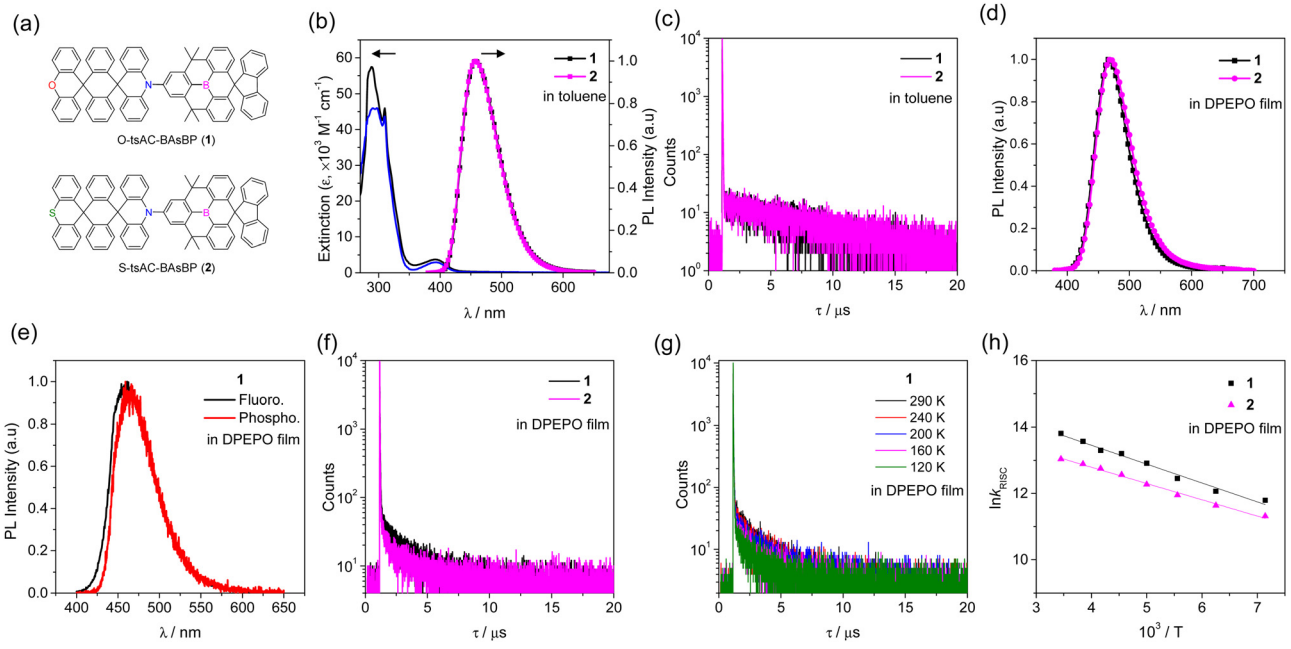

Fig. 1 (a) Chemical structures of **1** and **2**. (b) Absorption and PL spectra of **1** and **2** in toluene (c = 2.0 × 10^{-5} M, λ_{ex} = 310 nm). (c) Transient PL decay of **1** and **2** in toluene at 298 K. (d) PL spectra of 20 wt% doped films of **1** and **2** in a bis[2-(diphenylphosphino)phenyl]ether oxide (DPEPO) host. (e) Fluorescence and phosphorescence spectra of **1** and **2** at 77 K. (f) Transient PL decay of **1** and **2** at 298 K. (g) Temperature-dependent PL decay of **1**. (h) Arrhenius plots of k_{RISC} for **1** and **2**.

Table 1 Photophysical data and rate constants of **1** and **2**

Compound		λ_{abs} (nm)	λ_{PL} (nm)	Φ_{PL}[c] (%)	τ_p[d] (ns)	τ_d[d] (μs)	E_S/E_T[e] (eV)	ΔE_{ST}[f] (meV)	k_r[g] (10^7 s^{-1})	k_{ISC}[g] (10^7 s^{-1})	k_{RISC}[g] (10^5 s^{-1})	E_a[h] (meV)
O-tsAC-BAsBP (**1**)	sol[a]	394	457	70	20	5.83						
	Film[b]		467	100	16	1.55	2.89/2.86	35	4.06	2.23	9.99	15
S-tsAC-BAsBP (**2**)	sol[a]	395	457	74	20	7.50						
	Film[b]		469	84	14	1.98	2.95/2.90	50	4.68	1.57	6.86	13

[a] In N_2-filled toluene at 298 K ($c = 2.0 \times 10^{-5}$ M, λ_{ex} = 310 nm). [b] In 20 wt% doped films in a DPEPO host. [c] Absolute PLQYs. [d] Prompt (τ_p) and delayed (τ_d) PL decay lifetimes. [e] Singlet (E_S) and triplet (E_T) energy deduced from the onset of fluorescence and phosphorescence spectra at 77 K. [f] $\Delta E_{ST} = E_S - E_T$. [g] k_r, k_{ISC}, and k_{RISC} are the fluorescence radiative decay, intersystem crossing, and RISC rate constants, respectively. [h] Activation energies of RISC.

obtained at 77 K demonstrated an involvement of CT excited states in the emission, along with small ΔE_{ST} values of 0.035 eV for **1** and 0.050 eV for **2**, respectively (Fig. 1e and Fig. S12, ESI†).

Notably, the transient PL decays showed short-lived delayed fluorescence lifetimes (τ_d = 1.55–1.98 μs), which is in accordance with the very small ΔE_{ST} values (Fig. 1f). The delayed fluorescence intensities were gradually increased with an increase of temperature from 120 K to 290 K, confirming the TADF nature (Fig. 1g and Fig. S13, ESI†). The excited state dynamics of **1** and **2** were further understood by calculating the rate constants of intersystem crossing (k_{ISC}) and RISC (k_{RISC}) (Table 1).[37] The k_{ISC} and k_{RISC} values were estimated to be in the orders of $\sim 10^7$ and $\sim 10^6$ s^{-1}, respectively, for both compounds, indicating fast spin–flip processes.[38,39] The higher k_{RISC} of **1** than that of **2** was aligned with the shorter delayed fluorescence lifetime of **1**. The Arrhenius plots of k_{RISC} resulted in the very small activation energies of RISC (E_a^{RISC}), equal to 15 meV for **1** and 13 meV for **2** (Fig. 1h and Table 1). The similar tiny E_a^{RISC} values also supported the fast RISC process in **1** and **2**. Moreover, the values were smaller than the corresponding ΔE_{ST} values, indicating the involvement of the higher-lying T_2 state in the RISC process, accompanied by vibronic coupling between the T_1 and T_2 states.[40–42]

Theoretical studies

Density functional theory (DFT) and time-dependent DFT (TD-DFT) calculations were conducted using the PBE0 hybrid functional[43] and the 6-31+G(d,p) basis set to elucidate the molecular geometries and electronic structures of **1** and **2** in the ground and excited states. The energy differences between S_1 and T_1 states were computed using the Tamm–Dancoff approximation (TDA).[44,45] In the optimized molecular structures, the acridine donor and *B*-heterotriangulene acceptor fragments are connected in a highly twisted conformation with a large dihedral angle of $\sim 90^\circ$ owing to the steric hindrance caused by the acridine rings (Fig. S14, ESI†). The HOMO and LUMO are mainly distributed on the acridine donor and the *B*-heterotriangulene acceptor, respectively. The well-separated HOMO and LUMO resulted in very small ΔE_{ST} values of 11–12 meV, which aligns with the experimental results. Overall, the numerical values for the optimized structures of **1** and **2**, such as the dihedral angle, MO energy, HOMO–LUMO gap, ΔE_{ST}, and overlap integral ($I_{H/L}$) between the HOMO and the LUMO, were comparable for both compounds, accounting for their similar photophysical properties. This result can be attributed to the negligible contributions from the O- and S-containing ring fragments of the tsAC donor to the HOMO. Natural

Table 2 Natural transition orbitals (NTOs) for the excited states of **1** and **2** obtained using the TDDFT calculations at the PBE0/6-31+G(d,p) level of theory. The numerical values for spin–orbit coupling matrix elements and transition rates for the RISC processes are obtained using the PBE0/6-311G(d,p)//6-31+G(d,p) level of theory

1	Hole	Electron	**2**	Hole	Electron
T_2 (^3LE_A) (3.111 eV)	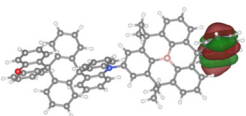	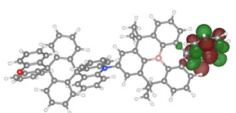	T_2 (^3LE_A) (3.107 eV)	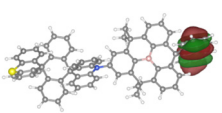	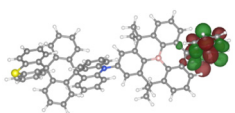
T_1 (^3CT) (2.726 eV)	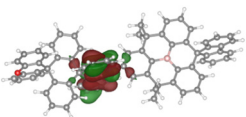	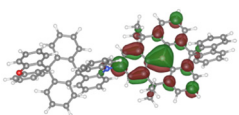	T_1 (^3CT) (2.731 eV)	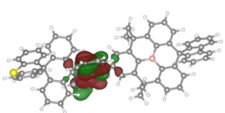	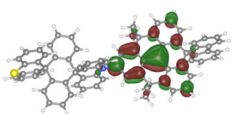
S_1 (^1CT) (2.737 eV)	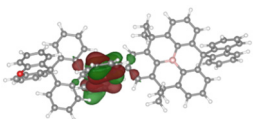	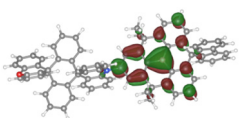	S_1 (^1CT) (2.743 eV)	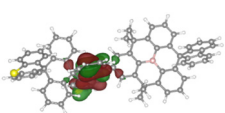	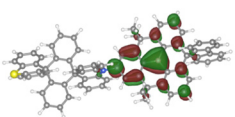
$\langle S_1\|\hat{H}_{SOC}\|T_1\rangle$	0.104 cm^{-1}		$\langle S_1\|\hat{H}_{SOC}\|T_1\rangle$	0.112 cm^{-1}	
$\langle S_1\|\hat{H}_{SOC}\|T_2\rangle$	0.380 cm^{-1}		$\langle S_1\|\hat{H}_{SOC}\|T_2\rangle$	0.369 cm^{-1}	
$k_{T_1\rightarrow S_1}$	5.86×10^5 s^{-1}		$k_{T_1\rightarrow S_1}$	6.00×10^5 s^{-1}	
$k_{T_2\rightarrow S_1}$	1.85×10^7 s^{-1}		$k_{T_2\rightarrow S_1}$	2.27×10^7 s^{-1}	

transition orbitals (NTOs) of **1** and **2** were examined to analyze the nature of the excited states (Table 2). The hole and electron NTOs of the S_1 and T_1 states are predominantly localized in the D and A units, respectively, which is indicative of the CT excited states (^{1}CT and ^{3}CT). This result is in good accordance with the fluorescence and phosphorescence spectra of **1** and **2** at 77 K (Fig. S12, ESI†). Due to the same CT nature of the S_1 and T_1 states, spin–orbit coupling (SOC) between the two states could be weak according to the El-Sayed rule.[41,46] Thus, we examined the NTOs of the next higher-lying triplet (T_2) state of **1** and **2** and found that both the hole and electron NTOs of the T_2 states are localized on the spiro-fluorenyl moiety in the BAsBP acceptor units, indicating an LE character (^3LE_A) of the T_2 states. To support the finding, we first analyzed the NTOs of the pristine D and A molecules (Fig. S15, ESI†). The T_1 states of X-tsACH (X = O, S) and HBAsBP are localized on the acridine ring and the spiro-fluorenyl moiety, respectively, with the lower computed T_1 energy level of HBAsBP (E_T(A) = 2.930 eV) compared to that of X-tsACH (E_T(D) = 3.131 eV). Next, we recorded the phosphorescence spectra of the pristine donor molecules at 77 K (Fig. S16, ESI†).

Both the X-tsACH donors showed the identical T_1 energy levels of 3.061 eV, higher than that of the HBAsBP acceptor molecule (^3LE_A = 2.877 eV).[30] These theoretical and experimental results confirm the ^3LE_A character of the T_2 states of **1** and **2**. Accordingly, the significant SOC matrix elements (SOCMEs) between the S_1 (^{1}CT) and T_2 (^{3}LE) states ($\langle S_1|\hat{H}_{SOC}|T_2\rangle$ = 0.369–0.380 cm^{-1}) were comparably obtained for **1** and **2** as anticipated by the El-Sayed rule (Table 2). The values were also over three times greater than those between the S_1 (^{1}CT) and T_1 (^{3}CT) states ($\langle S_1|\hat{H}_{SOC}|T_1\rangle$ = 0.104–0.112 cm^{-1}). Furthermore, the calculated RISC rate constants between the T_2 and S_1 states ($k_{T_2\rightarrow S_1}$ = 1.85–2.27 × 10^7 s^{-1}) were significantly higher than those between the T_1 and S_1 states ($k_{T_1\rightarrow S_1}$ = 5.86–6.00 × 10^5 s^{-1}). Therefore, these results highlight that the SOC between the T_2 and S_1 states can boost the rate of RISC in **1** and **2**, thereby supporting the observed high RISC rates.[38,47,48]

Electroluminescence properties

The electroluminescence (EL) performances of **1** and **2** as the TADF emitters were finally evaluated by fabricating blue OLEDs with the following device structures (Fig. 2a): glass/indium-tin-oxide (ITO, 70 nm)/molybdenum trioxide (MoO_3, 5 nm)/1,1-bis[(di-4-tolylamino)phenyl]cyclohexane (TAPC, 40 nm)/tris(4-carbazoyl-9-ylphenyl)amine (TCTA, 10 nm)/1,3-bis(*N*-carbazolyl) benzene (*m*CP, 10 nm)/DPEPO:emitter (10, 20 wt%, 25 nm)/DPEPO (5 nm)/2,2′,2″-(1,3,5-benzinetriyl)-tris(1-phenyl-1-*H*-benzimidazole) (TPBi, 35 nm)/lithium fluoride (LiF, 1 nm)/aluminum (Al, 100 nm). DPEPO was selected as the host material due to its high T_1 level (~3.0 eV) suitable for efficient energy transfer to the emitters.[5,49] We employed two different emitter concentrations (10 and 20 wt%) in the emissive layer to optimize the performances of TADF-OLEDs. The EL characteristics of the devices are summarized in Table 3 and Fig. 2b–d and Fig. S18 and S19, ESI.†

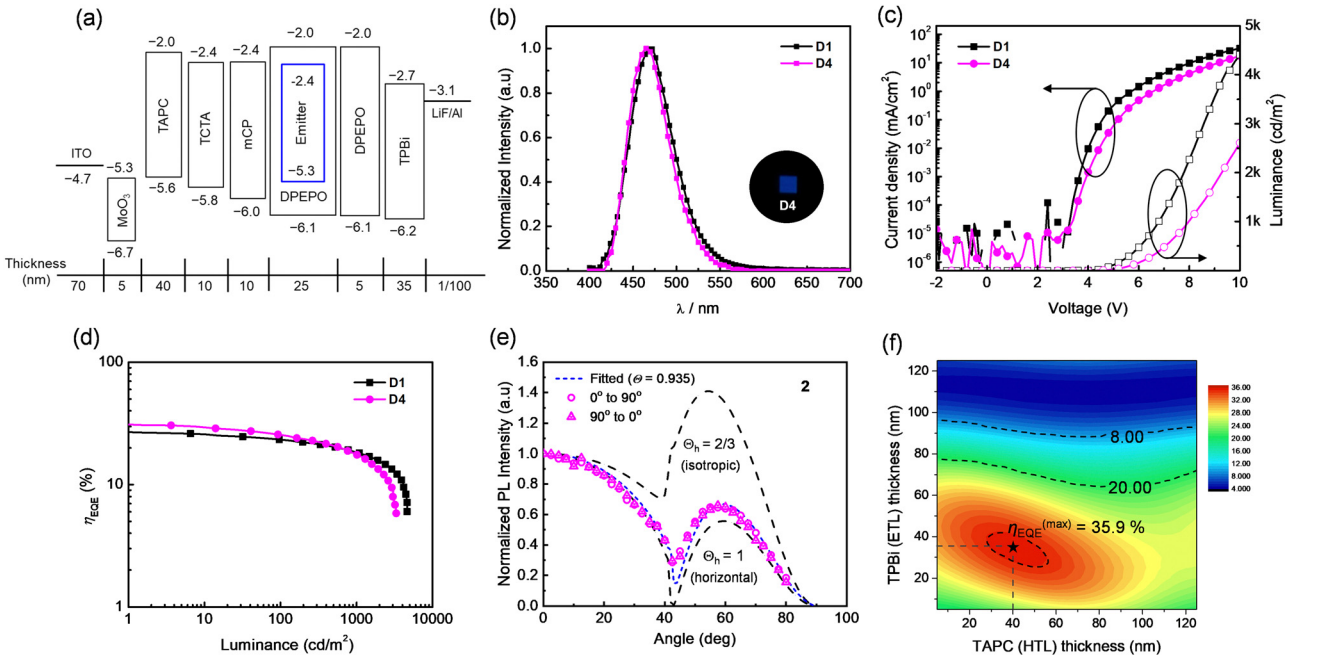

Fig. 2 (a) Device structure and energy level diagram (eV) of the TADF-OLEDs. (b) EL spectra of **D1** an **D4** and the photograph of the working **D4** device. (c) Current density–voltage–luminance (*J*–*V*–*L*) characteristics of **D1** and **D4**. (d) External quantum efficiency–luminance (η_{EQE}–*L*) characteristics of **D1** and **D4**. (e) Angle-dependent PL intensity of the emitting layer with emitter **2**. (f) The contour plot of the theoretical maximum EQEs for device **D4** as a function of the TPBi and TAPC thicknesses. The star symbol indicates the maximum EQE value for **D4**.

Table 3 Device characteristics of TADF-OLEDs

Device[a]	Emitter (wt%)	λ_{EL} (nm)	λ_{FWHM}[b] (nm)	CIE (x, y)[c]	V_{on}[d] (V)	EQE[e] (%)	PE[f] (lm W^{-1})	CE[g] (cd A^{-1})
D1	**1** (20)	469	58	(0.137, 0.147)	3.7	27.4/18.4	32.3/11.8	43.2/29.0
D2	**2** (20)	467	58	(0.133, 0.140)	3.8	24.7/16.6	25.0/9.6	32.7/22.0
D3	**1** (10)	465	57	(0.134, 0.108)	3.8	22.5/15.4	23.5/9.1	22.8/15.6
D4	**2** (10)	466	55	(0.132, 0.117)	4.0	31.5/17.6	30.2/8.4	44.0/24.6

[a] ITO (70 nm)/MoO_3 (5 nm)/TAPC (40 nm)/TCTA (10 nm)/mCP (10 nm)/DPEPO:emitter(10, 20 wt%, 25 nm)/DPEPO (5 nm)/TPBi (35 nm)/LiF (1 nm)/Al (100 nm). [b] Full width at half maximum (FWHM). [c] Color coordinates (CIE 1931) at a maximum luminance. [d] Applied voltage at a luminance of 1 cd m^{-2}. [e] External quantum efficiency: maximum, then the value at 1000 cd m^{-2}. [f] Maximum power efficiency: maximum, then the value at 1000 cd m^{-2}. [g] Maximum current efficiency: maximum, then the value at 1000 cd m^{-2}.

At 20 wt% doping concentration, devices **D1** and **D2** with emitters **1** and **2**, respectively, exhibited blue EL emissions centered at 469 and 467 nm, comparable to the PL spectra of the emitters doped in the host films. The CIE_y values for the EL emissions of the two devices fell within 0.15. Notably, **D1** and **D2** exhibited high maximum EQEs (EQE_{max}) of 27.4% for **D1** and 24.7% for **D2**, respectively, which are in accordance with the PLQYs of the emitters doped in the host films (Table 1). Meanwhile, for the 10 wt%-doped devices (**D3** and **D4**), the EL spectra underwent slight blue-shifts, showing the EL peaks at 465 and 466 nm, respectively. Along with the narrow FWHMs of 55–57 nm, the EL spectra led to the CIE_y values of ~0.11, corresponding to the deep-blue emission of the devices. It is noticeable that the observed FWHMs are slightly narrower than those obtained with previous emitter **3** (FWHM = 57–58 nm), presumably due to the increased molecular rigidity offered by the tri-spiral donor structure.[26] Remarkably, device **D4** with emitter **2** exhibited a very high EQE_{max} of 31.5%, although the EQE of **D3** based on **1** was somewhat reduced to 22.5% at the 10 wt% emitter concentration. To partly explain this result, we prepared 10 wt%-doped host films of **1** and **2** in a DPEPO host and measured their photophysical properties (Table S1, ESI†). Interestingly, the PLQY of the host film doped with **2** reached near-unity, while that with **1** exhibited 82%. Thus, the high EQE of **D4** could be understood with the increased PLQY of **2** at 10 wt% doping. Although the EQE_{max} values for the devices with **1** and **2** showed an opposite trend depending on the doping concentration of the emitters, the observed efficiencies could be ranked among the highest value for the deep-blue devices with D–A-type emitters ($CIE_y < 0.12$).[26,50–52] In addition, since the η_{out} is one of the important factors governing the EQE of a device, we estimated the $\Theta_{\parallel}$ of the doped host films of **1** and **2** utilizing angle-dependent PL measurements. As shown in Fig. 2e and Fig. S20 (ESI†), both films exhibited very high $\Theta_{\parallel}$ values of 93.0% and 93.5%, respectively. The values are higher than that of previous emitter **3** containing sAC and BAsBP units (~90%).[30] Therefore, the increased molecular length and rigidity, endowed by the tri-spiral donor and spiro-acceptor units, can be regarded beneficial for attaining high $\Theta_{\parallel}$ values, leading to the improved η_{out} of device and thereby enhancing the EQE of the device over 30%. To the best of our knowledge, the $\Theta_{\parallel}$ value of ~93% is the highest among the spiro,[16,18,21,24] bi-spiral,[24,50] or tri-spiral acridine donor-based emitters ($\Theta_{\parallel}$ = 88–90%).[15,26] The high device efficiency of **D4** was further elucidated by the optical simulations. Using the PLQY and $\Theta_{\parallel}$ of the emitter **2** and the OLED structure, the contour map of the theoretically achievable EQE_{max} values was obtained as illustrated in Fig. 2f. The resultant theoretical EQE_{max} was found to be 35.9% for the **D4** device, accounting for the observed high efficiency of **D4**.

Conclusions

We have demonstrated that linear-shaped D–A-type compounds, O-tsAC-BAsBP (**1**) and S-tsAC-BAsBP (**2**), which consisted of rigid tri-spiral acridine donor and spiro-fluorenyl-*B*-heterotriangulene acceptor units, can act as highly efficient deep-blue TADF emitters in OLEDs. Both the emitters doped into host films exhibited deep-blue emissions with outstanding TADF characteristics, such as a high PLQY of ~100%, a small ΔE_{ST} of less than 50 meV, and a short τ_d of ~2 μs. The RISC process was found to be accelerated by effective SOC between the ^{1}CT (S_1) and ^{3}LE (T_2) excited states, resulting in a rate constant of ~10^6 s^{-1}. Above all, the emitters displayed a remarkably high horizontal dipole orientation ratio ($\Theta_{\parallel}$) of ~93%. Thanks to their high PLQYs, $\Theta_{\parallel}$, and molecular rigidity, the optimized TADF-OLEDs incorporating emitters **1** and **2** achieved narrow deep-blue EL emissions with peak wavelengths of 465–469 nm, with EQE_{max} values as high as 27.4% (**1**) and 31.5% (**2**), respectively. The findings of this study are promising for the development of TADF emitters with a high horizontal dipole orientation, which can ultimately enhance the efficiency of OLEDs.

Conflicts of interest

There are no conflicts to declare.

Acknowledgements

This work was supported by the Basic Science Research Program funded by the Ministry of Science and ICT (MSIT) (NRF-2019R1A2C1084952 and NRF-2021R1A4A1027480 for M.H.L) and the Ministry of Education (NRF-2021R1A6A1A03038858) through the National Research Foundation of Korea (NRF). S. Yoo acknowledges the support from the Technology Innovation Program (20020408, Development of direct analytic methods for exciton dynamics in OLEDs and lifetime-enhancing technologies based thereon) funded by the Ministry of Trade,

Industry & Energy (MOTIE, Korea) through the Korea Evaluation Institute of Industrial Technology (KEIT).

References

1 X. Cai and S.-J. Su, Marching Toward Highly Efficient, Pure-Blue, and Stable Thermally Activated Delayed Fluorescent Organic Light-Emitting Diodes, *Adv. Funct. Mater.*, 2018, **28**, 1802558.
2 M. Y. Wong and E. Zysman-Colman, Purely Organic Thermally Activated Delayed Fluorescence Materials for Organic Light-Emitting Diodes, *Adv. Mater.*, 2017, **29**, 1605444.
3 H. Kaji, H. Suzuki, T. Fukushima, K. Shizu, K. Suzuki, S. Kubo, T. Komino, H. Oiwa, F. Suzuki, A. Wakamiya, Y. Murata and C. Adachi, Purely organic electroluminescent material realizing 100% conversion from electricity to light, *Nat. Commun.*, 2015, **6**, 8476.
4 Y. Tao, K. Yuan, T. Chen, P. Xu, H. Li, R. Chen, C. Zheng, L. Zhang and W. Huang, Thermally activated delayed fluorescence materials towards the breakthrough of organoelectronics, *Adv. Mater.*, 2014, **26**, 7931–7958.
5 Q. Zhang, B. Li, S. Huang, H. Nomura, H. Tanaka and C. Adachi, Efficient blue organic light-emitting diodes employing thermally activated delayed fluorescence, *Nat. Photonics*, 2014, **8**, 326–332.
6 F. B. Dias, K. N. Bourdakos, V. Jankus, K. C. Moss, K. T. Kamtekar, V. Bhalla, J. Santos, M. R. Bryce and A. P. Monkman, Triplet harvesting with 100% efficiency by way of thermally activated delayed fluorescence in charge transfer OLED emitters, *Adv. Mater.*, 2013, **25**, 3707–3714.
7 H. Uoyama, K. Goushi, K. Shizu, H. Nomura and C. Adachi, Highly efficient organic light-emitting diodes from delayed fluorescence, *Nature*, 2012, **492**, 234–238.
8 H. Nakanotani, T. Higuchi, T. Furukawa, K. Masui, K. Morimoto, M. Numata, H. Tanaka, Y. Sagara, T. Yasuda and C. Adachi, High-efficiency organic light-emitting diodes with fluorescent emitters, *Nat. Commun.*, 2014, **5**, 4016.
9 C. Mayr, S. Y. Lee, T. D. Schmidt, T. Yasuda, C. Adachi and W. Brütting, Efficiency Enhancement of Organic Light-Emitting Diodes Incorporating a Highly Oriented Thermally Activated Delayed Fluorescence Emitter, *Adv. Funct. Mater.*, 2014, **24**, 5232–5239.
10 K.-H. Kim, C.-K. Moon, J.-H. Lee, S.-Y. Kim and J.-J. Kim, Highly Efficient Organic Light-Emitting Diodes with Phosphorescent Emitters Having High Quantum Yield and Horizontal Orientation of Transition Dipole Moments, *Adv. Mater.*, 2014, **26**, 3844–3847.
11 S.-Y. Kim, W.-I. Jeong, C. Mayr, Y.-S. Park, K.-H. Kim, J.-H. Lee, C.-K. Moon, W. Brütting and J.-J. Kim, Organic Light-Emitting Diodes with 30% External Quantum Efficiency Based on a Horizontally Oriented Emitter, *Adv. Funct. Mater.*, 2013, **23**, 3896–3900.
12 D. Yokoyama, Molecular orientation in small-molecule organic light-emitting diodes, *J. Mater. Chem.*, 2011, **21**, 19187–19202.
13 Y. Lee and J.-I. Hong, High-efficiency thermally activated delayed fluorescence emitters via a high horizontal dipole ratio and controlled dual emission, *J. Mater. Chem. C*, 2020, **8**, 8012–8017.
14 Y. Xiang, P. Li, S. Gong, Y.-H. Huang, C.-Y. Wang, C. Zhong, W. Zeng, Z. Chen, W.-K. Lee, X. Yin, C.-C. Wu and C. Yang, Acceptor plane expansion enhances horizontal orientation of thermally activated delayed fluorescence emitters, *Sci. Adv.*, 2020, **6**, eaba7855.
15 W. Li, B. Li, X. Cai, L. Gan, Z. Xu, W. Li, K. Liu, D. Chen and S.-J. Su, Tri-Spiral Donor for High Efficiency and Versatile Blue Thermally Activated Delayed Fluorescence Materials, *Angew. Chem., Int. Ed.*, 2019, **58**, 11301–11305.
16 Y. Fu, H. Liu, D. Yang, D. Ma, Z. Zhao and B. Z. Tang, Boosting external quantum efficiency to 38.6% of sky-blue delayed fluorescence molecules by optimizing horizontal dipole orientation, *Sci. Adv.*, 2021, **7**, eabj2504.
17 I. S. Park, H. Min, J. U. Kim and T. Yasuda, Deep-Blue OLEDs Based on Organoboron–Phenazasiline-Hybrid Delayed Fluorescence Emitters Concurrently Achieving 30% External Quantum Efficiency and Small Efficiency Roll-Off, *Adv. Opt. Mater.*, 2021, **9**, 2101282.
18 G. Xia, C. Qu, Y. Zhu, J. Ye, K. Ye, Z. Zhang and Y. Wang, A TADF Emitter Featuring Linearly Arranged Spiro-Donor and Spiro-Acceptor Groups: Efficient Nondoped and Doped Deep-Blue OLEDs with CIEy <0.1, *Angew. Chem., Int. Ed.*, 2021, **60**, 9598–9603.
19 W. Li, M. Li, W. Li, Z. Xu, L. Gan, K. Liu, N. Zheng, C. Ning, D. Chen, Y.-C. Wu and S.-J. Su, Spiral Donor Design Strategy for Blue Thermally Activated Delayed Fluorescence Emitters, *ACS Appl. Mater. Interfaces*, 2021, **13**, 5302–5311.
20 W. Li, W. Li, L. Gan, M. Li, N. Zheng, C. Ning, D. Chen, Y.-C. Wu and S.-J. Su, J-Aggregation Enhances the Electroluminescence Performance of a Sky-Blue Thermally Activated Delayed-Fluorescence Emitter in Nondoped Organic Light-Emitting Diodes, *ACS Appl. Mater. Interfaces*, 2020, **12**, 2717–2723.
21 T.-A. Lin, T. Chatterjee, W.-L. Tsai, W.-K. Lee, M.-J. Wu, M. Jiao, K.-C. Pan, C.-L. Yi, C.-L. Chung, K.-T. Wong and C.-C. Wu, Sky-Blue Organic Light Emitting Diode with 37% External Quantum Efficiency Using Thermally Activated Delayed Fluorescence from Spiroacridine-Triazine Hybrid, *Adv. Mater.*, 2016, **28**, 6976–6983.
22 H. Peng, Y. Xu, C. Zhou, R. Pei, J. Miao, H. Liu and C. Yang, Donor Extension on Spiro-Acridine Enables Highly Efficient TADF-OLEDs with Relieved Efficiency Roll-Off, *Adv. Funct. Mater.*, 2023, **33**, 2211696.
23 S. Xiao, Y. Gao, R. Wang, H. Liu, W. Li, C. Zhou, S. Xue, S.-T. Zhang, B. Yang and Y. Ma, Highly efficient hybridized local and Charge-transfer (HLCT) Deep-blue electroluminescence with excellent molecular horizontal orientation, *Chem. Eng. J.*, 2022, **440**, 135911.
24 H. Lim, H. J. Cheon, S.-J. Woo, S.-K. Kwon, Y.-H. Kim and J.-J. Kim, Highly Efficient Deep-Blue OLEDs using a TADF Emitter with a Narrow Emission Spectrum and High Horizontal Emitting Dipole Ratio, *Adv. Mater.*, 2020, **32**, 2004083.

25 X. Gong, P. Li, Y.-H. Huang, C.-Y. Wang, C.-H. Lu, W.-K. Lee, C. Zhong, Z. Chen, W. Ning, C.-C. Wu, S. Gong and C. Yang, A Red Thermally Activated Delayed Fluorescence Emitter Simultaneously Having High Photoluminescence Quantum Efficiency and Preferentially Horizontal Emitting Dipole Orientation, *Adv. Funct. Mater.*, 2020, **30**, 1908839.
26 Y. Lee and J.-I. Hong, High-Efficiency Thermally Activated Delayed Fluorescence Emitters with High Horizontal Orientation and Narrow Deep-Blue Emission, *Adv. Opt. Mater.*, 2021, **9**, 2100406.
27 R. Pei, J. Lou, G. Li, H. Liu, X. Yin, C. Zhou, Z. Wang and C. Yang, Modulating LUMO extension of Spiro-junction TADF emitters for efficient OLEDs with relieved efficiency Roll-Off, *Chem. Eng. J.*, 2022, **437**, 135222.
28 J. Rao, C. Zhao, Y. Wang, K. Bai, S. Wang, J. Ding and L. Wang, Achieving Deep-Blue Thermally Activated Delayed Fluorescence in Nondoped Organic Light-Emitting Diodes through a Spiro-Blocking Strategy, *ACS Omega*, 2019, **4**, 1861–1867.
29 T. Nakagawa, S.-Y. Ku, K.-T. Wong and C. Adachi, Electroluminescence based on thermally activated delayed fluorescence generated by a spirobifluorene donor–acceptor structure, *Chem. Commun.*, 2012, **48**, 9580–9582.
30 Y. H. Lee, W. Lee, T. Lee, J. Jung, S. Yoo and M. H. Lee, Achieving over 36% EQE in blue OLEDs using rigid TADF emitters based on spiro-donor and spiro-B-heterotriangulene acceptors, *Chem. Eng. J.*, 2023, **452**, 139387.
31 Y. H. Lee, W. Lee, T. Lee, D. Lee, J. Jung, S. Yoo and M. H. Lee, Blue TADF Emitters Based on B-Heterotriangulene Acceptors for Highly Efficient OLEDs with Reduced Efficiency Roll-Off, *ACS Appl. Mater. Interfaces*, 2021, **13**, 45778–45788.
32 C. M. Hsieh, T. L. Wu, J. Jayakumar, Y. C. Wang, C. L. Ko, W. Y. Hung, T. C. Lin, H. H. Wu, K. H. Lin, C. H. Lin, S. Hsieh and C. H. Cheng, Diboron-Based Delayed Fluorescent Emitters with Orange-to-Red Emission and Superior Organic Light-Emitting Diode Efficiency, *ACS Appl. Mater. Interfaces*, 2020, **12**, 23199–23206.
33 I. S. Park, K. Matsuo, N. Aizawa and T. Yasuda, High-Performance Dibenzoheteraborin-Based Thermally Activated Delayed Fluorescence Emitters: Molecular Architectonics for Concurrently Achieving Narrowband Emission and Efficient Triplet–Singlet Spin Conversion, *Adv. Funct. Mater.*, 2018, **28**, 1802031.
34 J. U. Kim, I. S. Park, C.-Y. Chan, M. Tanaka, Y. Tsuchiya, H. Nakanotani and C. Adachi, Nanosecond-time-scale delayed fluorescence molecule for deep-blue OLEDs with small efficiency rolloff, *Nat. Commun.*, 2020, **11**, 1765.
35 R. Ishimatsu, S. Matsunami, K. Shizu, C. Adachi, K. Nakano and T. Imato, Solvent Effect on Thermally Activated Delayed Fluorescence by 1,2,3,5-Tetrakis(carbazol-9-yl)-4,6-dicyanobenzene, *J. Phys. Chem. A*, 2013, **117**, 5607–5612.
36 X. Tang, L.-S. Cui, H.-C. Li, A. J. Gillett, F. Auras, Y.-K. Qu, C. Zhong, S. T. E. Jones, Z.-Q. Jiang, R. H. Friend and L.-S. Liao, Highly efficient luminescence from space-confined charge-transfer emitters, *Nat. Mater.*, 2020, **19**, 1332–1338.
37 K.-C. Pan, S.-W. Li, Y.-Y. Ho, Y.-J. Shiu, W.-L. Tsai, M. Jiao, W.-K. Lee, C.-C. Wu, C.-L. Chung, T. Chatterjee, Y.-S. Li, K.-T. Wong, H.-C. Hu, C.-C. Chen and M.-T. Lee, Efficient and Tunable Thermally Activated Delayed Fluorescence Emitters Having Orientation-Adjustable CN-Substituted Pyridine and Pyrimidine Acceptor Units, *Adv. Funct. Mater.*, 2016, **26**, 7560–7571.
38 Y. Wada, H. Nakagawa, S. Matsumoto, Y. Wakisaka and H. Kaji, Organic light emitters exhibiting very fast reverse intersystem crossing, *Nat. Photonics*, 2020, **14**, 643–649.
39 L.-S. Cui, A. J. Gillett, S.-F. Zhang, H. Ye, Y. Liu, X.-K. Chen, Z.-S. Lin, E. W. Evans, W. K. Myers, T. K. Ronson, H. Nakanotani, S. Reineke, J.-L. Bredas, C. Adachi and R. H. Friend, Fast spin-flip enables efficient and stable organic electroluminescence from charge-transfer states, *Nat. Photonics*, 2020, **14**, 636–642.
40 T. J. Penfold, E. Gindensperger, C. Daniel and C. M. Marian, Spin-Vibronic Mechanism for Intersystem Crossing, *Chem. Rev.*, 2018, **118**, 6975–7025.
41 M. K. Etherington, J. Gibson, H. F. Higginbotham, T. J. Penfold and A. P. Monkman, Revealing the spin–vibronic coupling mechanism of thermally activated delayed fluorescence, *Nat. Commun.*, 2016, **7**, 13680.
42 J. Gibson, A. P. Monkman and T. J. Penfold, The Importance of Vibronic Coupling for Efficient Reverse Intersystem Crossing in Thermally Activated Delayed Fluorescence Molecules, *Chem. Phys. Chem.*, 2016, **17**, 2956–2961.
43 C. Adamo and V. Barone, Toward reliable density functional methods without adjustable parameters: The PBE0 model, *J. Chem. Phys.*, 1999, **110**, 6158–6170.
44 M. Moral, L. Muccioli, W. J. Son, Y. Olivier and J. C. Sancho-García, Theoretical Rationalization of the Singlet–Triplet Gap in OLEDs Materials: Impact of Charge-Transfer Character, *J. Chem. Theory Comput.*, 2015, **11**, 168–177.
45 S. Hirata and M. Head-Gordon, Time-dependent density functional theory within the Tamm–Dancoff approximation, *Chem. Phys. Lett.*, 1999, **314**, 291–299.
46 S. K. Lower and M. A. El-Sayed, The Triplet State and Molecular Electronic Processes in Organic Molecules, *Chem. Rev.*, 1966, **66**, 199–241.
47 H. Noda, X.-K. Chen, H. Nakanotani, T. Hosokai, M. Miyajima, N. Notsuka, Y. Kashima, J.-L. Brédas and C. Adachi, Critical role of intermediate electronic states for spin-flip processes in charge-transfer-type organic molecules with multiple donors and acceptors, *Nat. Mater.*, 2019, **18**, 1084–1090.
48 F. B. Dias, J. Santos, D. R. Graves, P. Data, R. S. Nobuyasu, M. A. Fox, A. S. Batsanov, T. Palmeira, M. N. Berberan-Santos, M. R. Bryce and A. P. Monkman, The Role of Local Triplet Excited States and D–A Relative Orientation in Thermally Activated Delayed Fluorescence: Photophysics and Devices, *Adv. Sci.*, 2016, **3**, 1600080.

49 C. Han, Y. Zhao, H. Xu, J. Chen, Z. Deng, D. Ma, Q. Li and P. Yan, A Simple Phosphine–Oxide Host with a Multi-insulating Structure: High Triplet Energy Level for Efficient Blue Electrophosphorescence, *Chem. – Eur. J.*, 2011, **17**, 5800–5803.
50 T. Hua, Y.-C. Liu, C.-W. Huang, N. Li, C. Zhou, Z. Huang, X. Cao, C.-C. Wu and C. Yang, High-efficiency and low roll-off deep-blue OLEDs enabled by thermally activated delayed fluorescence emitter with preferred horizontal dipole orientation, *Chem. Eng. J.*, 2022, **433**, 133598.
51 D. H. Ahn, S. W. Kim, H. Lee, I. J. Ko, D. Karthik, J. Y. Lee and J. H. Kwon, Highly efficient blue thermally activated delayed fluorescence emitters based on symmetrical and rigid oxygen-bridged boron acceptors, *Nat. Photonics*, 2019, **13**, 540–546.
52 P. Rajamalli, N. Senthilkumar, P.-Y. Huang, C.-C. Ren-Wu, H.-W. Lin and C.-H. Cheng, New Molecular Design Concurrently Providing Superior Pure Blue, Thermally Activated Delayed Fluorescence and Optical Out-Coupling Efficiencies, *J. Am. Chem. Soc.*, 2017, **139**, 10948–10951.